Mapping differential interactomes by affinity purification coupled with data-independent mass spectrometry acquisition

Jean-Philippe Lambert[1,13], Gordana Ivosev[2,13], Amber L Couzens[1], Brett Larsen[1], Mikko Taipale[3], Zhen-Yuan Lin[1], Quan Zhong[4–6], Susan Lindquist[3,7,8], Marc Vidal[4–6], Ruedi Aebersold[9,10], Tony Pawson[1,11,12], Ron Bonner[2], Stephen Tate[2] & Anne-Claude Gingras[1,11]

Characterizing changes in protein-protein interactions associated with sequence variants (e.g., disease-associated mutations or splice forms) or following exposure to drugs, growth factors or hormones is critical to understanding how protein complexes are built, localized and regulated. Affinity purification (AP) coupled with mass spectrometry permits the analysis of protein interactions under near-physiological conditions, yet monitoring interaction changes requires the development of a robust and sensitive quantitative approach, especially for large-scale studies in which cost and time are major considerations. We have coupled AP to data-independent mass spectrometric acquisition (sequential window acquisition of all theoretical spectra, SWATH) and implemented an automated data extraction and statistical analysis pipeline to score modulated interactions. We used AP-SWATH to characterize changes in protein-protein interactions imparted by the HSP90 inhibitor NVP-AUY922 or melanoma-associated mutations in the human kinase CDK4. We show that AP-SWATH is a robust label-free approach to characterize such changes and propose a scalable pipeline for systems biology studies.

Protein-protein interactions (PPIs) are essential to cellular functions and are attractive therapeutic intervention targets[1,2]. PPIs are also becoming increasingly recognized for their potential in contributing to disease phenotypes induced by genetic variations, including splice variants, allelic variants and point mutations[3–6]. Systematic assessment of the consequences of sequence variation on protein-protein interactions by yeast two-hybrid (Y2H) assays has revealed clear interaction changes associated with disease-associated mutants[7]. However, PPI screening with only Y2H analysis generates results that do not easily capture quantitative differences in interaction potential and that work best to highlight interactions that are lost rather than *de novo* interactions that may be gained via sequence variation.

AP coupled with mass spectrometry (AP-MS) can identify interactions in near-physiological conditions, providing proper functional context to the studied protein modules[8]. Although many groups have employed AP-MS to identify static interactomes, very few publications have focused on the identification of differential interactions; in all cases, these studies have employed quantitative proteomics, with or without isotopes, to discriminate between condition-specific interactions (reviewed in refs. 9,10). Notably, in these studies, MS acquisition was performed in a data-dependent manner (data-dependent acquisition, DDA), in which peptides to be sequenced are selected on the basis of the relative abundance of their precursor-ion signals. DDA introduces a degree of stochasticity in this process, which makes it very difficult to conclude that a peptide or protein is truly absent in a given sample, especially for lower-abundance species[11,12]. This is especially problematic for comparative quantification[10].

In recent years, a different paradigm for MS-based quantification of proteins has gained increased acceptance. Quantification using MS/MS (MS2) increases specificity and signal-to-noise ratios as compared to precursor ions (MS1). This is the basis behind selected reaction monitoring (SRM), also known as multiple reaction monitoring, which has been efficiently coupled to affinity purification, thereby permitting the detailed analysis of dynamic signaling modules[13,14]. The utility of SRM in the quantification of AP samples is highlighted by its simplicity, accuracy and sensitivity[15]. Because SRM quantification does not rely on the measured abundance of the precursor ion in MS1, there is a decreased chance of missing values in the data set. However, SRM requires a substantial investment in assay development for each peptide of interest[16]. Furthermore, the list of analyzed peptide species is predetermined,

which precludes a posteriori reanalysis of this type of data as new information becomes available, and the number of peptides quantified per liquid chromatography–MS/MS run is limited.

The advantages of quantification at the level of MS2 may also be harnessed in another type of acquisition strategy, namely data-independent acquisition (DIA[17]; reviewed in ref. 12). In DIA, precursor ions are fragmented independently of their signal in MS1. A type of DIA that is particularly promising for the analysis of AP samples is termed SWATH[18]. In SWATH, the entire useful mass range is scanned in a cycle time compatible with liquid chromatography using wide mass-isolation windows. All precursors in each window are fragmented, which results in an MS2 map of all compounds. A list of peptide fragment masses (for example, acquired by a parallel DDA experiment) is used to correlate MS2 peaks within the data set to specific peptides, a step allowing quantification as in SRM data. The method benefits from many of the same attributes as SRM, such as high throughput and accuracy of quantification[18,19], and possesses a dynamic range compatible with even the most complex interaction proteomics experiments (see the accompanying paper by Collins et al.[20]). Here we present a complete experimental and computational pipeline that couples AP with SWATH quantification.
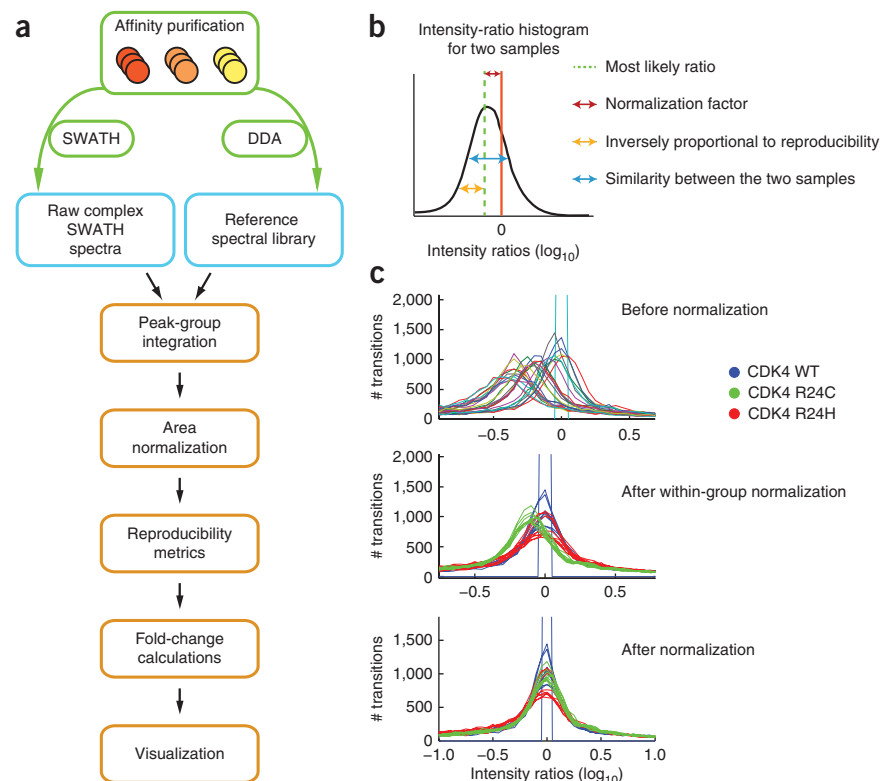
RESULTS
A pipeline for quantitative interactome monitoring

SWATH uses a fast-scanning triple quadrupole time-of-flight (QQQTOF) mass spectrometer[21] to systematically fragment all ions within a given m/z range. Eluting peptide precursor ions are isolated in sequential, slightly overlapping windows of 25 atomic mass units (a.m.u.) (for 100 ms per window) and fragmented. The composite MS/MS spectra for all coeluting and co-isolated precursors are recorded as a complete fragment-ion map of the sample studied (**Supplementary Fig. 1**). As previously reported[18], quantification of SWATH data can be accomplished by targeted data extraction using a list of fragment masses (see, for example, ref. 18).

To analyze our AP samples, we purified each of the bait samples in biological replicates using Flag magnetic beads, and peptides were prepared by tryptic digestion. Each of the biological replicates was analyzed by SWATH. We generated reference spectral libraries for targeted extraction by analyzing at least one biological replicate for each of the groups of samples by DDA (**Fig. 1a**, **Supplementary Tables 1** and **2** and Online Methods). The DDA samples generated across a complete data set were collectively searched using the ProteinPilot software, and the MS2 spectra matching peptide sequences were used to create a reference list of fragment masses for high-confidence hits (Online Methods). This library was used to interrogate each SWATH run, enabling peptide quantification across all SWATH samples, even if a given peptide was not identified in the matched DDA run. The PeakView SWATH Processing Micro App (AB Sciex) was used to identify the correct peak group in a set of fragment chromatograms with peaks at the same retention time (**Supplementary Fig. 1c,e**). Peak-group scoring was similar to that described previously[18] and used a combination of chromatographic correlation (related peaks should have the same shape, width and retention time), mass error and additional predicted fragments ions; a decoy strategy was used to select most likely peak groups for export and quantitative analysis (Online Methods and **Supplementary Fig. 1d**).

Because of the amount of data generated by the SWATH approach and the goal of minimizing manual processing, we developed a statistical method to calculate fold-change values and evaluate the confidence of these calculations. We perform normalization by calculating the most likely ratio between pairs of samples (Online Methods), which generates a scaling factor and metrics about the similarity of the samples and the quality of the measurements. Normalization is applied stepwise, first to the samples that are expected to be most similar (replicates)

Figure 1 | AP-SWATH pipeline. (**a**) MS analysis pipeline: each sample is processed separately for DDA and SWATH, and the spectral library built from all DDA runs within an experimental set is used to retrieve quantitative information from each of the SWATH runs. A series of tools is used to automatically match the DDA and SWATH spectra; extract quantitative information; normalize the transitions, peptides and proteins; and determine the fold-change differences between samples and the confidence of the fold change. (**b**) Schematic of the parameters used for normalization. Intensity-ratio histograms are generated between pairs of samples, and a number of metrics are derived. (**c**) Effects of the normalization steps on the area-ratio histograms demonstrated for a data set consisting of nine samples each derived from CDK4 WT, CDK4 R24C and CDK4 R24H. Top, ratio histograms before normalization; center, after normalization based on experimental types (here biological replicates); and bottom, final results after normalization of the experimental bias.

Figure 2 | AP-SWATH for scoring protein interactions. (**a**) Reproducibility metrics for the SWATH extraction at 1% FDR in relation to the binned % CV values; the upper boundary is indicated, and values ≤20% CV are shaded. (**b**) Reproducibility metrics for the common peptides identified in all DDA experiments and extracted from SWATH data with 1% FDR. The numbers of peptides and proteins identified or quantified within the % CV indicated are plotted, and the overall percentages of peptides and proteins within the 20% CV interval are indicated. (**c**) Fold-change calculation results for the Flag-EIF4A2 bait in relation to a negative control, Flag-GFP (left) and for Flag-MEPCE in relation to Flag-GFP (right). The proteins that changed at least twofold with a confidence of ≥0.75 are displayed: increased proteins (yellow scale) are specific to the bait in relation to the control, whereas the decreased proteins (blue scale) are more abundant in the negative-control samples and likely are contaminants (these tend to be enriched in the contaminant repository for affinity purification[38], http://crapome.org/). Proteins preferentially associating with the negative control are labeled in red. Several components of well-characterized protein complexes that were enriched with EIF4A2 and MEPCE are indicated by the colored dots to the right of the heat maps (see **Supplementary Figs. 9–11** for an expanded view). snRNP complex, small nuclear ribonucleoprotein complex. In this and all other heat maps, values exceeding the fold change ($\log_{10}$) indicated in the color-coding bars are depicted as the maximal intensity values.
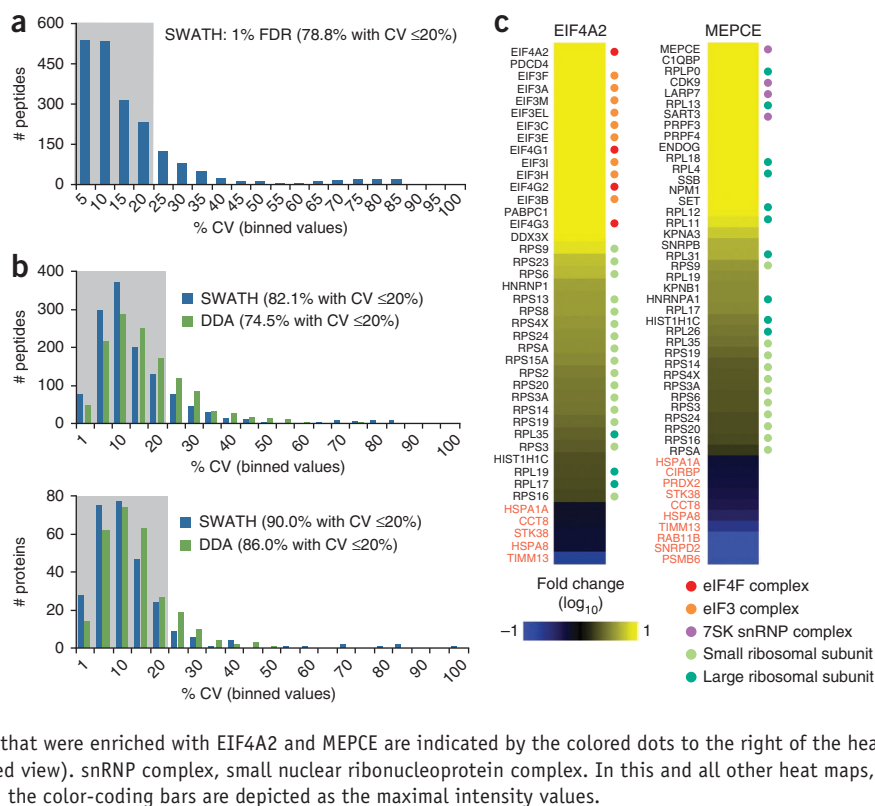
and then to the different sample groups (**Fig. 1b,c**). The quality metrics are combined with signal metrics, such as signal-to-noise ratio, and used as weights in calculating fold-change values using a strategy first described for the analysis of SRM data for AP samples[13] and referred to here as fold-change calculation. With this approach, poor-quality measurements are downweighted, which removes the need to manually reject samples or measurements or to perform outlier rejection. Essentially, this statistical tool evaluates the quality of each measurement using weights based on reproducibility (results for each data set used here are in **Supplementary Figs. 2–7**) and performs fold-change calculation of pairwise samples at the level of transitions, peptides and proteins (Online Methods).

To determine whether the automated method yielded reproducible data, we measured the variance for all quantifiable peptides (with peak-group false discovery rate (FDR) ≤1%; **Supplementary Fig. 8**) on a data set consisting of cyclin-dependent kinase CDK4 AP samples derived from three biological replicates and analyzed in parallel by DDA and by SWATH (additionally, three technical replicates were acquired for each biological replicate for SWATH). SWATH data extraction led to quantification of 79% peptides within coefficient of variation (CV) of 20% (**Fig. 2a**), resulting in 87% of proteins with ≤20% CV. These results were compared to MS1 area measurements extracted using ProteinPilot software from the DDA data of the same replicates and were used to determine the level of both stochasticity and variance in the measurement between samples. 5,089 peptides were identified in any of the three DDA runs with an ID confidence ≥99%, but only 2,741 were common to all three DDA runs with an ID confidence ≥99% in at least one of the replicates. These values highlight the issues of stochasticity associated with DDA data. For comparison with the

SWATH results, calculation of variance was performed on only the 1,320 high-confidence peptides identified in all DDA runs and with ≤1% peak group FDR in the SWATH data. SWATH had a higher proportion (82.1% versus 74.5%) of peptides detected with CV ≤20% and also a smaller variance at the protein level (**Fig. 2b**). Notably, however, SWATH had the same reproducibility for extraction of peptides targeted across all samples. From these studies, we conclude that our extraction and normalization pipeline for SWATH data is reliable (see Online Methods for additional benchmarking measures), and we next benchmarked it on AP samples.

To test whether the automated pipeline could reproduce known interactions in complex AP samples, we tested it for measuring interactions for well-characterized baits, namely, EIF4A2 and MEPCE, which we compared to a negative control (GFP fused to a 3xFlag tag). Here and throughout the manuscript, all proteins were stably expressed in the Flp-In T-REx system (Life Technologies), which enabled recombinant protein expression to be driven in a tetracycline-inducible manner from a single locus. N-terminal 3xFlag tags permit purification on Flag M2 magnetic beads, and purification was followed by on-bead tryptic digestion as previously described[22]. The resulting peptides were analyzed by DDA and SWATH in triplicates. Following analysis by our automated pipeline, we observed that known interaction partners of EIF4A2 and MEPCE showed large fold change (≥2) in expression over that of the GFP control (**Fig. 2c** and **Supplementary Figs. 9–11**). In fact, the relative fold-change values detected for EIF4A2 (a component of the trimeric eIF4F complex) mirrored the known assembly of the preinitiation machinery in human cells[23]. The highest fold-change values were detected for the bait, after the bait were PDCD4 (a known negative regulator of EIF4A2 that binds

Figure 3 | Selected biological samples. (**a**) Schematic representation of the effects of mutations, splice variants and chemical perturbations on the modulation of specific protein-protein interactions. In the reference interactome, interaction of the central protein with three binding partners is represented. If this protein is absent from the cells, all three interactions are lost (blue interactome; node removal). Interactions can also be selectively lost (green interactome, edge lost) or gained (red interactome, edge gain). In these cases, the loss or gain can be absolute (represented here by the presence or absence of an edge) or partial (depicted by changes in edge thickness; the magnitude of these changes can be measured by quantitative proteomics). (**b**) AP-western validation of a test case for monitoring interactome changes. Flag-tagged CDK4 WT and mutant proteins are expressed at similar amounts (to each other and to the endogenous CDK4 protein) in Flp-In T-REx 293 cells and purified on an anti-Flag resin. Association of the endogenous p18INK (CDKN2C) protein was detected by immunoblotting.

to the bait directly[24]) and the other components of eIF4F and the eIF3 complex (which are tethered to EIF4A2 via direct association to eIF4G proteins). Next on the enrichment list were many of the components of the 40S ribosomal subunit, which is recruited to EIF4A2 via the eIF3 complex; very few of the 60S ribosomal subunits were detected confidently—that is, with at least twofold higher expression than that of the GFP control—a result consistent with the fact that this subunit assembles onto the 48S preinitiation complex only when translation is poised. Similarly, MEPCE, the methylphosphate-capping enzyme for 7SK RNAs, associated most strongly with components of the 7SK small nuclear ribonucleoprotein complex[25], followed by splicing components and several components of the 60S ribosomal subunit, which were in this case enriched in preference to the 40S ribosomal components. In summary, after scoring based on the comparison to negative control samples, the AP-SWATH pipeline is robust, reproducible and amenable to interactome mapping.

AP-SWATH rapidly identifies differential interactomes

We were interested here not only in scoring protein interactions over a negative control but also in systematically monitoring interactome changes in pairs of samples (either sequence variants or drug-treated samples; **Fig. 3a**). We elected to study a well-described series of sequence variants for CDK4 that has been identified in melanoma patients[26,27]. Structurally, mutation at Arg24 precludes association of CDK4 with a family of polypeptide inhibitors, the INK proteins (p15INK, p16INK, p18INK and p19INK[28]; **Supplementary Table 1**), resulting in derepressed CDK4 activity and accelerated cellular proliferation[7,29]. We first demonstrated that the sequence variants behaved as expected by performing AP and western blotting (AP-western) with antibodies directed against known endogenous partners. All recombinant proteins were expressed at levels similar to each other and to the endogenous CDK4 (**Fig. 3b**). As expected, CDK4 wild type (WT), but not the two mutants (R24C and R24H), interacted with p18INK (CDKN2C) (**Fig. 3b**). These samples—and a negative control—were chosen to explore quantification by the AP-SWATH method.

Principal-component analysis (PCA) of the data from the four tested sample pairs revealed clear separation of the negative controls from any of the baits (**Fig. 4a**). 17 proteins were enriched at least twofold in one of the three CDK4 baits: these were deemed CDK4 interactors (**Fig. 4b** and **Supplementary Figs. 12–14**). To assess how these interactors were associating with either of the two mutants in relation to the WT protein (clearly separated by PCA;
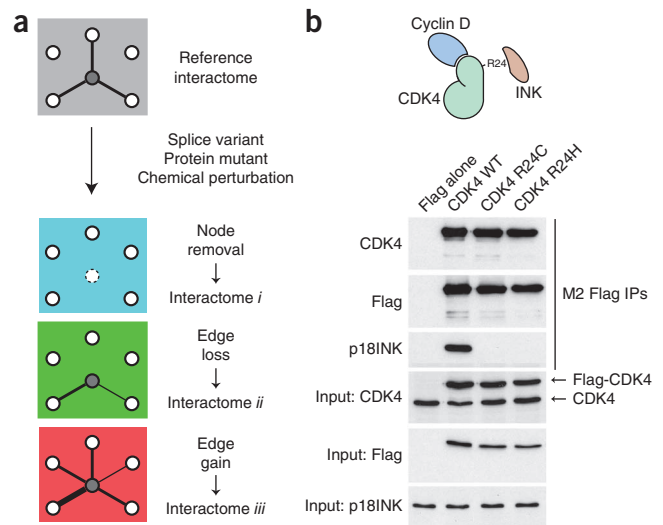
Fig. 4a), we implemented a stringent two-step filtering approach. Only CDK4 interactors (as per **Fig. 4b**) were considered in an additional test to assess confidence of a change (up or down in this case; we set an arbitrary threshold at twofold; **Fig. 4c**). When using the pipeline described above to characterize interactions for the CDK4 proteins, we observed a number of differentially regulated interactions between the WT and the two mutant proteins (R24C and R24H). In contrast, the two mutants shared most interactions (**Fig. 4d** and **Supplementary Fig. 15**). As expected, both mutants largely lost interactions with members of the INK family of CDK inhibitors (5.7- to 9.8-fold reduction; **Fig. 4d** and **Supplementary Figs. 15–17**; see Online Methods for the inclusion criteria). However, we also noticed a pronounced increase in the association of HSP90 proteins (HSP90AA1 and HSP90AB1; ≥3.0-fold) and the CDC37 co-chaperone (≥3.9-fold) with the two mutant proteins. In addition, the immunophilin FKBP51 (encoded by *FKBP4*) and, to a lesser extent, HSP70 (encoded *HSPA8*) were also substantially enriched in the mutants. To further cross-validate these results, we performed an additional series of CDK4 AP coupled with isobaric tags for relative and absolute quantitation (iTRAQ) labeling (**Fig. 4d**) and extracted abundance ratios for the ten proteins modulated in the R24 mutants as compared to the WT. The iTRAQ measurements revealed modulation consistent with SWATH for these ten proteins (**Fig. 4d**), though the variance associated with iTRAQ measurements was considerably higher (**Supplementary Fig. 18**), at least in part owing to stochasticity between independent iTRAQ runs. The regulated interactions with CDC37 and HSP90 were validated by AP-western analysis, which confirmed the trends observed by AP-SWATH (**Fig. 4e**). Taken together, this indicated a higher propensity of the mutant proteins to interact with HSP90 and suggested that the enriched interactors may be recruited to CDK4 via interactions with HSP90 core components. However, these effects were not observed to the same extent with two other CDK4 mutants, for which interaction with the INK proteins is not modulated (N41S and S52N; **Supplementary Figs. 19–22**), suggesting some degree of specificity in the recruitment of HSP90 to CDK4 mutants at Arg24. In summary, the AP-SWATH method enabled confirmation of known regulated interactions and quantification of the changes, and it permitted the discovery of new modulated interactions.
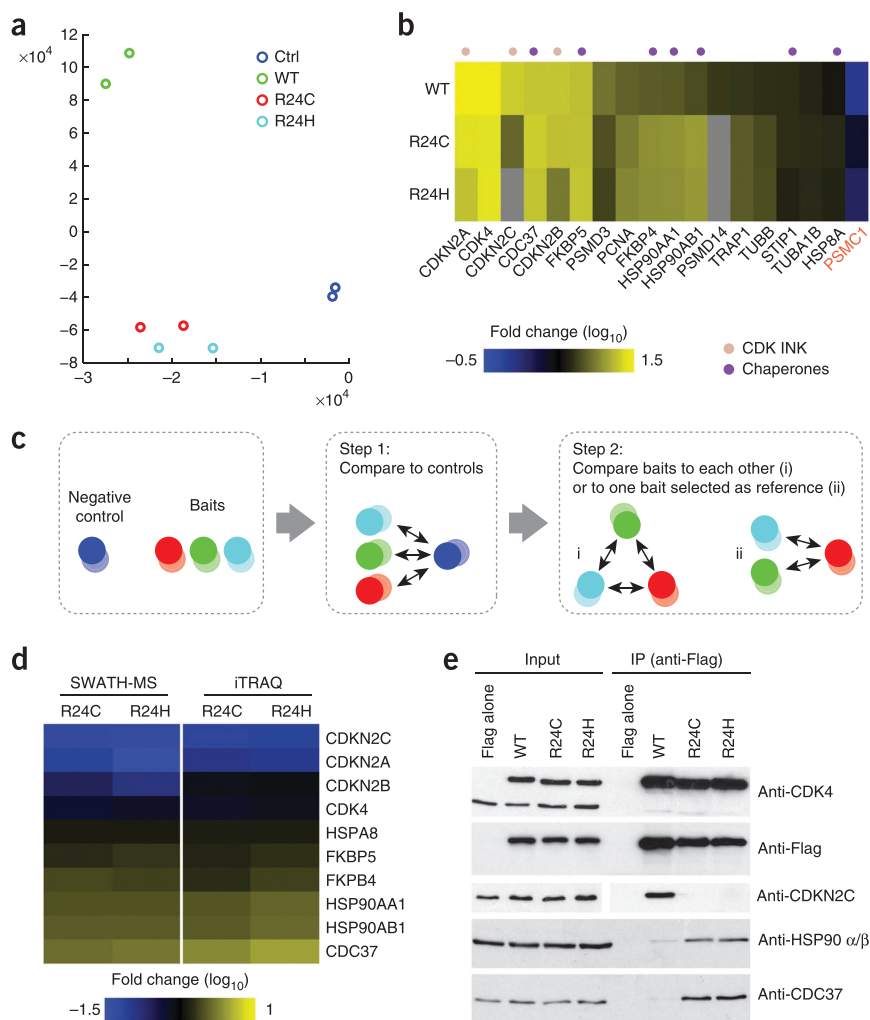
Figure 4 | Identification of differential interactomes for CDK4 cancer-associated mutants. (**a**) Principal-component analysis showing the clear separation of two control (Ctrl; Flag alone) samples and two WT CDK4 samples in comparison to the two R24 CDK4 samples, which show little separation from one another. (**b**) Heat map representation of the proteins passing the confidence threshold in one of the CDK4 baits relative to the negative controls. The gray cells indicate that the thresholds for confidence, fold change or signal-to-noise ratio were not met in this particular pairwise comparison (see **Supplementary Fig. 12** for a global view of all the data without these missing values and **Supplementary Figs. 13** and **14** for expanded views). (**c**) Schematic of the scoring process for differential interactome mapping. In the first step, the potential interactions for a set of baits are collectively scored against a negative control, and proteins confidently upregulated with at least one bait are considered further. In the second step, systematic pairwise comparisons between all baits, or comparison to a bait used as a reference point, are performed. (**d**) Left, heat map depicting the high-confidence proteins differentially detected in the R24C and R24H mutants in relation to the WT sample. Only proteins changing with a confidence ≥0.75 and passing filtering criteria (Online Methods) are depicted. See **Supplementary Figures 15–17** for all pairwise comparisons. Right, heat map showing the iTRAQ ratios of the high-confidence SWATH proteins (see **Supplementary Fig. 18** for iTRAQ ratio s.d.). (**e**) Validation of selected regulated interactions by AP-western. IP, immunoprecipitation.

AP-SWATH can identify drug-regulated interactions

Although increased interaction between CDK4 mutants and HSP90 has never been reported, mutations in several other kinases (including EGFR and BRAF) increase their interaction with CDC37 and HSP90 (refs. 30,31). This result was recapitulated here using a luminescence-based mammalian interactome (LUMIER) approach (as in ref. 32; **Fig. 5a** and **Supplementary Fig. 23**). A model of addiction to HSP90 has been proposed, in which mutant kinases become dependent on CDC37-HSP90 folding for stability and activity[33], offering a rationale for the use of HSP90 inhibitors that prevent the recruitment of client proteins as a therapeutic avenue. Using AP-SWATH we thus assessed the consequences on recruitment of CDC37 and HSP90 to the kinase constructs following treatment with NVP-AUY922 (a potent HSP90 inhibitor currently undergoing a clinical trial[34]). We also reasoned that proteins that were displaced at the same time as CDC37 and HSP90 may be dependent on the interaction with the core HSP90 network for their interactions.

As expected, treatment of the cells expressing CDK4 WT with the HSP90 inhibitor resulted in marked dissociation of CDC37 and HSP90 (**Fig. 5b**,**c** and **Supplementary Figs. 24–27**). Many of the proteins that showed increased association with the mutant proteins as compared to WT were also affected in their interactions with the NVP-AUY922 treatment, a result indicating that

they are likely mediated by the CDC37-HSP90 bridge. Some other partners, however, including the chaperone HSP70 (encoded by *HSPA1A* and *HSPA8*) and some of its cofactors (HOP (*STIP1*) and HIP (*ST13*))[35], interacted more strongly with CDK4 WT in the presence of the inhibitor, which suggests that not only are these partners not recruited via CDC37-HSP90 but that they may compete with them for binding (**Fig. 5c**). Notably, and in contrast to the report that other mutant kinases show increased sensitivity for HSP90 inhibitors[30,31,36], we found that association of CDC37, HSP90 and FKBP4 to the mutant kinases was less affected than that to the WT following inhibitor treatment (**Fig. 5c**). Because the mutants also bound significantly more to these proteins in the absence of treatment (**Fig. 4**), this results in a much larger net binding in the presence of the inhibitor. Similarly, HSP90 almost completely dissociated from the WT CDK4 upon NVP-AUY922 treatment, whereas mutant CDK4 still associated with substantial amounts of the chaperone (**Fig. 5d**,**e**). We further explored this effect by performing time-course and dose-dependence analysis of the dissociation of the interactions. In all cases, association of the mutants with HSP90 and CDC37 was preserved as compared to the WT kinase, with longer treatment or higher dosages required for the dissociation of the CDK4 R24 mutants (**Fig. 5f**,**g** and **Supplementary Fig. 28**). Taken together, these results indicate that tumors driven by CDK4 oncogenic kinases may not benefit

Figure 5 | Use of AP-SWATH to probe drug-modulated interactions. (**a**) Increased association of kinase mutants with HSP90 as determined by a luminescence-based mammalian interactome (LUMIER) assay. Wild-type and mutant kinases are shown with their corresponding HSP90 interaction scores and s.d. (**b**) Heat map depicting the high-confidence differentially recovered proteins as a consequence of NVP-AUY922 (NVP) treatment (all comparisons are pairwise, for the same bait treated with NVP in comparison to the mock-treated sample (with DMSO, dimethylsulfoxide)). See **Supplementary Figure 24** for the heat map of the first filtering step (normalization to the negative control) and **Supplementary Figure 25** for an expanded view. (**c**) Fold change and median absolute variance (error bars) for all proteins from **b**. See **Supplementary Figures 26** and **27** for an expanded view of protein and peptide level changes. (**d**) Fold change and median absolute variance (error bars) of selected proteins in the mutants as compared to the WT following NVP treatment. (**e**) Validation of selected regulated interactions by AP-western: 500 nM NVP was used for 1 h. (**f**,**g**) AP-western analysis of the time course of CDK4 WT (**f**) and R24C mutant (**g**) dissociation from CDC37-HSP90 in the presence of 100 nM NVP. In **e**, **f** and **g**, * indicates the position of the Flag-tagged bait protein; • indicates endogenous CDK4.
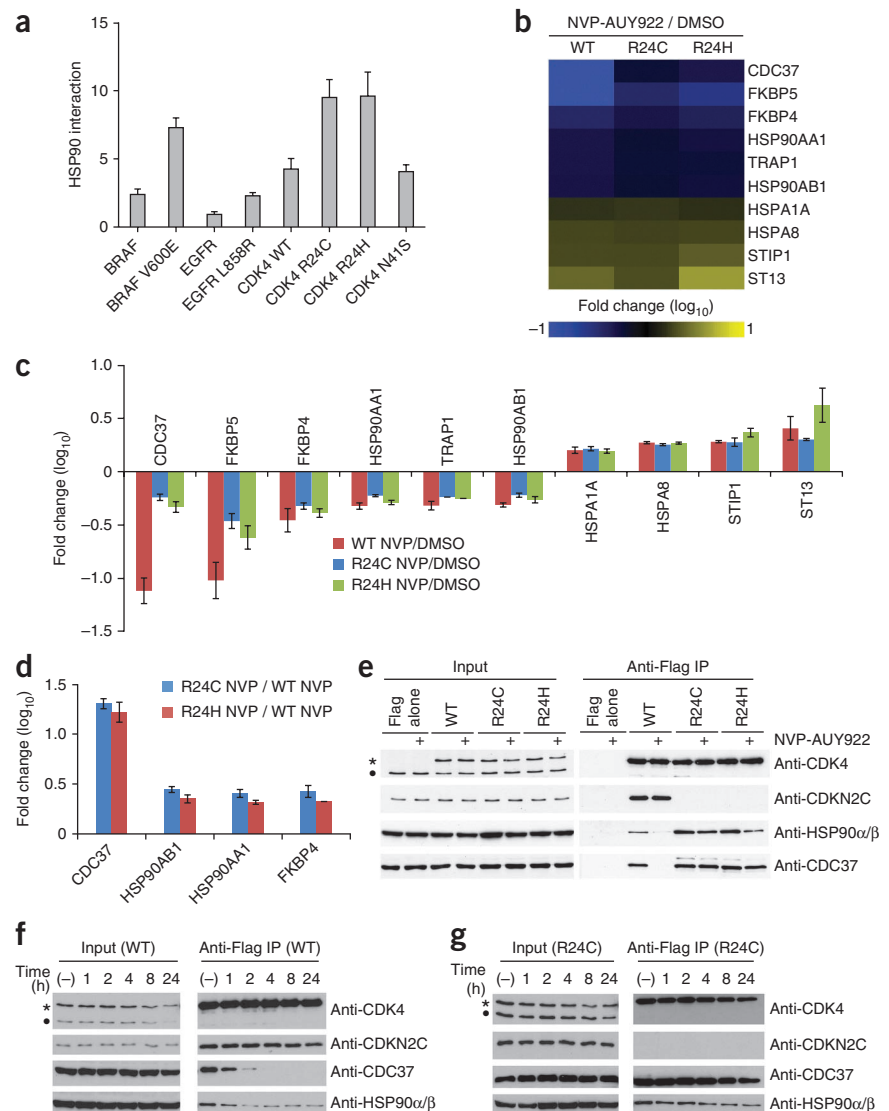
from treatment with HSP90 inhibitors or may require higher dosages to obtain the desired therapeutic results. Furthermore, our experiments set the stage for analyzing other drug-regulated interactions, including for other kinase oncogenic variants.

DISCUSSION

Here we report the development of an efficient pipeline to quantitatively study changes in interactomes in an unbiased and reproducible manner. Key aspects of the method are an unbiased DIA method, SWATH, and the use of weighted statistics to determine changes and associated confidence values. The latter is critical because it allows automatic analysis of the large amounts of data that can be generated in these experiments.

We have also shown that AP-SWATH is able to identify true interaction partners by scoring against negative-control samples and can rapidly identify interaction changes for disease-associated mutations and/or pharmacological treatment. As detailed in **Supplementary Figures 29–32**, the method is generally applicable, and we have implemented it to analyze the consequences on the interactome of alternative splicing, this time using three splice variants for another kinase, GRK6 (ref. 32; **Supplementary Discussion**). In all the cases we analyzed in more detail, the changes could be validated by AP-western analysis or iTRAQ quantitation. In this issue of *Nature Methods*, Collins *et al.* also report the use of AP-SWATH for monitoring the dynamics of association of 567 high-confidence 14-3-3β interaction partners[20], demonstrating that the approach can be used with even the most complex APs. Although the specifics of the data analysis approach are different

for the two papers (in particular, we introduce here a robust method of data normalization as part of the fold-change calculations; **Fig. 1b,c**), both manuscripts clearly demonstrate that AP-SWATH is appropriate for the analysis of interactome changes.

As for all targeting methods, the key for SWATH quantification is the generation of a spectral library. This can be provided from publicly available resources (as in ref. 18) but can also be built for a particular set of proteins of interest. Here we generated a spectral library from DDA data collected from the analysis of samples in each experimental set. We also note that samples could, for example, be pooled for the DDA identification run, and libraries could be built (as in ref. 18) for extracting the quantitative information. As there are a number of efforts to further understand the limits of DIA and SWATH and to evaluate ways to build libraries, it is likely that new ways to analyze the data will become available. In fact, this is a key strength of the DIA approach: the data generated provide a permanent record of the whole sample, enabling future reanalysis. In combination with proper data annotation (for example, using laboratory information management systems such as ProHits[37]) and deposition in public repositories (as we have done here with MassIVE), this should provide an important source of information for computational and cancer biologists alike.

METHODS
Methods and any associated references are available in the online version of the paper.

Note: Any Supplementary Information and Source Data files are available in the online version of the paper.

AUTHOR CONTRIBUTIONS
J.-P.L. generated all CDK4 samples and performed validation experiments; G.I. developed the pipeline for the normalization and fold-change calculation and performed statistical analysis; A.L.C. generated all GRK6 samples and performed validation experiments; M.T. performed LUMIER analysis and provided constructs; Z.-Y.L. prepared samples for mass spectrometry; B.L. and S.T. performed mass spectrometric measurements and iTRAQ data analysis; Q.Z. and M.V. provided initial constructs and input on the project; S.L. supervised M.T., and T.P. cosupervised J.-P.L.; R.A., R.B. and S.T. co-developed the SWATH approach; J.-P.L., A.L.C., B.L., A.-C.G., G.I. and S.T. analyzed the SWATH data; A.-C.G. wrote the manuscript with input from all authors; A.-C.G. conceived of the study and directed the project.

COMPETING FINANCIAL INTERESTS
The authors declare competing financial interests: details are available in the online version of the paper.

Reprints and permissions information is available online at http://www.nature.com/reprints/index.html.

1. Barrios-Rodiles, M. *et al.* High-throughput mapping of a dynamic signaling network in mammalian cells. *Science* **307**, 1621–1625 (2005).
2. Delmore, J.E. *et al.* BET bromodomain inhibition as a therapeutic strategy to target c-Myc. *Cell* **146**, 904–917 (2011).
3. Vacic, V. & Iakoucheva, L.M. Disease mutations in disordered regions—exception to the rule? *Mol. Biosyst.* **8**, 27–32 (2012).
4. Steward, R.E., MacArthur, M.W., Laskowski, R.A. & Thornton, J.M. Molecular basis of inherited diseases: a structural perspective. *Trends Genet.* **19**, 505–513 (2003).
5. Lahiry, P., Torkamani, A., Schork, N.J. & Hegele, R.A. Kinase mutations in human disease: interpreting genotype-phenotype relationships. *Nat. Rev. Genet.* **11**, 60–74 (2010).
6. Schuster-Böckler, B. & Bateman, A. Protein interactions in human genetic diseases. *Genome Biol.* **9**, R9 (2008).
7. Zhong, Q. *et al.* Edgetic perturbation models of human inherited disorders. *Mol. Syst. Biol.* **5**, 321 (2009).
8. Gingras, A.C., Gstaiger, M., Raught, B. & Aebersold, R. Analysis of protein complexes using mass spectrometry. *Nat. Rev. Mol. Cell Biol.* **8**, 645–654 (2007).
9. Ideker, T. & Krogan, N.J. Differential network biology. *Mol. Syst. Biol.* **8**, 565 (2012).
10. Gingras, A.C. & Raught, B. Beyond hairballs: the use of quantitative mass spectrometry data to understand protein-protein interactions. *FEBS Lett.* **586**, 2723–2731 (2012).
11. Tabb, D.L. *et al.* Repeatability and reproducibility in proteomic identifications by liquid chromatography-tandem mass spectrometry. *J. Proteome Res.* **9**, 761–776 (2010).
12. Tate, S., Larsen, B., Bonner, R. & Gingras, A.C. Label-free quantitative proteomics trends for protein-protein interactions. *J. Proteomics* **81**, 91–101 (2013).
13. Bisson, N. *et al.* Selected reaction monitoring mass spectrometry reveals the dynamics of signaling through the GRB2 adaptor. *Nat. Biotechnol.* **29**, 653–658 (2011).
14. Zheng, Y. *et al.* Temporal regulation of EGF signalling networks by the scaffold protein Shc1. *Nature* **499**, 166–171 (2013).
15. Picotti, P. & Aebersold, R. Selected reaction monitoring-based proteomics: workflows, potential, pitfalls and future directions. *Nat. Methods* **9**, 555–566 (2012).
16. Addona, T.A. *et al.* Multi-site assessment of the precision and reproducibility of multiple reaction monitoring-based measurements of proteins in plasma. *Nat. Biotechnol.* **27**, 633–641 (2009).
17. Venable, J.D., Dong, M.Q., Wohlschlegel, J., Dillin, A. & Yates, J.R. Automated approach for quantitative analysis of complex peptide mixtures from tandem mass spectra. *Nat. Methods* **1**, 39–45 (2004).
18. Gillet, L.C. *et al.* Targeted data extraction of the MS/MS spectra generated by data-independent acquisition: a new concept for consistent and accurate proteome analysis. *Mol. Cell. Proteomics* **11**, O111.016717 (2012).
19. Liu, Y. *et al.* Quantitative measurements of N-linked glycoproteins in human plasma by SWATH-MS. *Proteomics* **13**, 1247–1256 (2013).
20. Collins, B.C. *et al.* Quantifying protein interaction dynamics by SWATH mass spectrometry: application to the 14-3-3 system. *Nat. Methods* doi:10.1038/nmeth.2703 (27 October 2013).
21. Andrews, G.L., Simons, B.L., Young, J.B., Hawkridge, A.M. & Muddiman, D.C. Performance characteristics of a new hybrid quadrupole time-of-flight tandem mass spectrometer (TripleTOF 5600). *Anal. Chem.* **83**, 5442–5446 (2011).
22. Kean, M.J., Couzens, A.L. & Gingras, A.C. Mass spectrometry approaches to study mammalian kinase and phosphatase associated proteins. *Methods* **57**, 400–408 (2012).
23. Gingras, A.C., Raught, B. & Sonenberg, N. eIF4 initiation factors: effectors of mRNA recruitment to ribosomes and regulators of translation. *Annu. Rev. Biochem.* **68**, 913–963 (1999).
24. Yang, H.S. *et al.* The transformation suppressor Pdcd4 is a novel eukaryotic translation initiation factor 4A binding protein that inhibits translation. *Mol. Cell. Biol.* **23**, 26–37 (2003).
25. Jeronimo, C. *et al.* Systematic analysis of the protein interaction network for the human transcription machinery reveals the identity of the 7SK capping enzyme. *Mol. Cell* **27**, 262–274 (2007).
26. Wölfel, T. *et al.* A p16INK4a-insensitive CDK4 mutant targeted by cytolytic T lymphocytes in a human melanoma. *Science* **269**, 1281–1284 (1995).
27. Zuo, L. *et al.* Germline mutations in the p16INK4a binding domain of CDK4 in familial melanoma. *Nat. Genet.* **12**, 97–99 (1996).
28. Serrano, M., Hannon, G.J. & Beach, D. A new regulatory motif in cell-cycle control causing specific inhibition of cyclin D/CDK4. *Nature* **366**, 704–707 (1993).
29. Coleman, K.G. *et al.* Identification of CDK4 sequences involved in cyclin D1 and p16 binding. *J. Biol. Chem.* **272**, 18869–18874 (1997).
30. Shimamura, T., Lowell, A.M., Engelman, J.A. & Shapiro, G.I. Epidermal growth factor receptors harboring kinase domain mutations associate with the heat shock protein 90 chaperone and are destabilized following exposure to geldanamycins. *Cancer Res.* **65**, 6401–6408 (2005).
31. Grbovic, O.M. *et al.* V600E B-Raf requires the Hsp90 chaperone for stability and is degraded in response to Hsp90 inhibitors. *Proc. Natl. Acad. Sci. USA* **103**, 57–62 (2006).
32. Taipale, M. *et al.* Quantitative analysis of Hsp90-client interactions reveals principles of substrate recognition. *Cell* **150**, 987–1001 (2012).
33. Prodromou, C. Strategies for stalling malignancy: targeting cancer's addiction to Hsp90. *Curr. Top. Med. Chem.* **9**, 1352–1368 (2009).
34. Brough, P.A. *et al.* 4,5-Diarylisoxazole Hsp90 chaperone inhibitors: potential therapeutic agents for the treatment of cancer. *J. Med. Chem.* **51**, 196–218 (2008).
35. Taipale, M., Jarosz, D.F. & Lindquist, S. HSP90 at the hub of protein homeostasis: emerging mechanistic insights. *Nat. Rev. Mol. Cell Biol.* **11**, 515–528 (2010).
36. da Rocha Dias, S. *et al.* Activated B-RAF is an Hsp90 client protein that is targeted by the anticancer drug 17-allylamino-17-demethoxygeldanamycin. *Cancer Res.* **65**, 10686–10691 (2005).
37. Liu, G. *et al.* ProHits: integrated software for mass spectrometry–based interaction proteomics. *Nat. Biotechnol.* **28**, 1015–1017 (2010).
38. Mellacheruvu, D. *et al.* The CRAPome: a contaminant repository for affinity purification–mass spectrometry data. *Nat. Methods* **10**, 730–736 (2013).

ONLINE METHODS

Generation of stable cell lines and drug treatment. We constructed the vector pDEST-5′Triple-Flag-pcDNA5-FRT-TO from the pcDNA5-FRT-Flag vector[39] and pMX-pie-pDEST-3X-Flag[40] by first preparing a HindIII/XhoI cassette from pMX-pie-pDEST-3X-Flag by PCR using the following oligos: 5′ ccttggAAGCTT CCACCATGGACTACAAAGACCATGACGG and 3′ ggactt CTCGAGtcagACCACTTTGTACAAGAAAGCTGAAC. This cassette was then subcloned into the pcDNA5-FRT-Flag vector (previously digested with HindIII/XhoI). Entry clones of wild-type and cancer-derived allelic series for the cyclin-dependent kinase CDK4 (c70t, g71a, a122g and g155a; all expressed in nucleotide base-pair changes, resulting in the expression of mutants R24C, R24H, N41S and S52N, respectively) were previously described[7]. Three splice variants of the GPCR-coupled receptor kinase GRK6 (variants A, B and C that differ in only their C-terminal extension; **Supplementary Fig. 29a**) were as previously reported[32]. Each entry clone was shuffled into the destination vector pDEST-5′Triple-Flag-pcDNA5-FRT-TO through homologous recombination using LR Clonase II (Gateway system; Invitrogen). The resulting vectors were cotransfected with the pOG44 recombinase in Flp-In T-REx HEK 293 (Invitrogen, grown in DMEM supplemented with 5% FBS, 5% calf serum, 100 U/mL penicillin/streptomycin) using Lipofectamine (Invitrogen) as per supplier instructions. pcDNA5-Flag-MEPCE and pcDNA-Flag-EIF4A2 were as previously described[39]. Cells stably expressing the constructs were selected in 200 μg/mL hygromycin for approximately 2 weeks, at which point cell colonies were pooled and expanded in 150-mm plates. (Cells have not been recently checked for mycoplasma contamination.) Once approximately 70% confluence was reached, we added tetracycline to a final concentration of 200 ng/mL to cell medium for 24 h, inducing the expression of the recombinant tagged protein. For experiments involving HSP90 inhibition, the HSP90 inhibitor NVP-AUY922 (ref. 34) (20 mM stock in DMSO) was added for the indicated times and inhibitor concentrations to cells previously induced with tetracycline for 24 h.

Affinity purification for mass spectrometry and validation by immunoblotting. Affinity purification was performed as previously described[22] with minor modifications. Briefly, cells expressing Flag-tagged proteins were washed with 10 mL of PBS before being scraped in PBS using a rubber spatula. Cells from two 150-mm plates were pelleted by centrifugation, the supernatant was removed, and cells were frozen on dry ice and kept frozen at −80 °C until used. Cells were lysed by resuspension in a 1:4 (pellet weight:volume) ratio of lysis buffer (50 mM HEPES-KOH (pH 8.0), 100 mM KCl, 2 mM EDTA, 0.1% NP40, 10% glycerol, 1 mM PMSF, 1 mM DTT and protease inhibitor cocktail (Sigma-Aldrich; P8340; 1:500)) followed by two freeze-thaw cycles. The resulting cell extract was then clarified by centrifugation at 20,800g for 20 min (4 °C) before the supernatant was transferred to a fresh tube. We performed affinity purifications performed by incubating the cleared lysate with 30 μL of prewashed magnetic M2 anti-Flag beads (Sigma-Aldrich) for 2 h at 4 °C on a nutator. Two washes with 1 mL of lysis buffer were then performed and followed by an additional wash with 1 mL of 20 mM Tris-HCl, pH 8, and 2 mM CaCl$_2$. For mass spectrometry analysis, 7.5 μL of 20 mM Tris-HCl, pH 8, containing 750 ng of trypsin (Sigma-Aldrich) was added to the washed beads and incubated at 37 °C for approximately 15 h. The next morning, the tubes were quickly centrifuged, the beads magnetized and the partially digested sample transferred to a fresh tube before addition of an extra 2.5 μL of 20 mM Tris-HCl, pH 8, containing 250 ng of trypsin. The samples were incubated for 3 h at 37 °C before addition of 1 μL of 50% formic acid. The samples were stored at −80 °C until analysis. For western blot analysis, the beads were resuspended in 2× Laemmli sample buffer and boiled for 5 min, and then the samples transferred were to fresh tubes. Proteins were separated by SDS-PAGE and transferred onto nitrocellulose membranes. For CDK4, the membranes were blocked in TBS containing 5 mg/mL nonfat milk and 1% Tween 20 for 1 h at room temperature. Blots were treated with primary and secondary antibodies as described in **Supplementary Table 3**: detection was performed by chemiluminescence detection with the LumiGLO reagent (Cell Signaling Technology; #7003; 1:20) on film. For GRK6, the membranes were blocked in 5% nonfat milk for 30 min at room temperature and then treated with primary antibodies overnight, followed by incubation for 1.5 h with IRDye 800CW anti-mouse and IRDye 680 anti-rabbit secondary antibodies (shown in **Supplementary Table 3**). The GRK6 membranes were then visualized by direct fluorescence scanning with a Li-Cor Odyssey Imager. HSP90 bands were quantified with Li-Cor Odyssey software.

LUMIER analysis. LUMIER analysis[1] was performed essentially as described in ref. 32. Briefly, wild-type kinases and indicated mutants C-terminally tagged with 3xFlag and V5 tags were transiently transfected in a 96-well format into 293T cells stably expressing *Renilla* luciferase–tagged HSP90β (encoded by *HSP90AB*). After passive lysis (in 50 mM HEPES-KOH, pH 7.9, 150 mM NaCl, 20 mM Na$_2$MoO$_4$, 2 mM EDTA, 5% glycerol, 0.5% Triton X-100, supplemented with protease and phosphatase inhibitors), the lysate was transferred into 384-well plates precoated with anti-Flag M2 (Sigma-Aldrich) and incubated for 3 h, which was followed by extensive washing and reaction with a *Gaussia* luciferase Flex kit (New England BioLabs). Subsequently, we detected the levels of the Flag-tagged bait by ELISA using HRP-conjugated anti-Flag antibody. Data analysis was performed as described in ref. 32.

Data sets used. This manuscript contains several data sets, organized in groups as detailed in **Supplementary Table 2**. For **Figures 1** and **2a,b**, the CDK4 WT runs from a set containing nine SWATH replicates (three biological × three technical) and three DDA replicates (three biological) were employed (group 5 in **Supplementary Table 2**). We randomized samples by ensuring that replicates were not run sequentially. For **Figure 2c**, the data set consisted of three biological replicates of each of the following: MEPCE, EIF4A2 and a GFP negative control (group 6). **Figure 4a,b** employed two biological replicates each of DMSO-treated CDK4 WT, R24C, R24H and an empty vector negative control (partial selection from group 3). **Figure 4d** (left) employed three biological replicates for the CDK4 WT, R24C and R24H mutants from group 1, whereas the right subpanel was from the iTRAQ data set in group 7. **Figure 5** used the entire HSP90 inhibitor data set (group 3). Data sets groups 2 and 4 were used for **Supplementary Figures 20–22** and **29–32**, respectively.

iTRAQ labeling. For validation of SWATH-MS results, an extra set of triplicate purifications of CDK4 samples were processed as described above except that HEPES buffer was substituted for Tris buffer during trypsin digestion, and samples were not acidified following tryptic digestion. Rather, the peptides were dried in a SpeedVac without heat and subsequently resuspended in 5 µL of iTRAQ dissolution buffer (as per the manufacturer, AB-Sciex, protocol). 20 µL of the appropriate iTRAQ reagent (from a stock solution of 50 µL in isopropanol) was added to each sample. Samples were labeled as follows: 3xFlag-GFP control (115), 3xFlag CDK4 WT (116), 3xFlag-CDK4 R24C (118) and 3xFlag-CDK4 R24H (119). After completion of the labeling reaction (2 h at room temperature), equal volumes of samples from individual biological replicates were mixed and evaporated to dryness in a SpeedVac. The dry peptides were resolubilized in 5% formic acid solution in water and one-eighth of the labeled peptides was used per MS analysis. This corresponded to loading twice as many peptides (in relation to the starting material) on the column as in the SWATH experiments.

Mass spectrometry data acquisition. Samples were analyzed on an AB Sciex 5600 TripleTOF in two phases: data-dependent acquisition (DDA) was followed by SWATH acquisition on the same sample, with the same gradient conditions and the same amounts of sample used (in most cases; detailed in **Supplementary Table 2**, DDA was performed on a single biological replicate, except for data sets 5 and 6, for which three DDA runs per bait were generated). For DDA, a quarter of the volume of the digested sample was analyzed on a 5600 TripleTOF using a Nanoflex cHiPLC system at 200 nL/min (Eksigent ChromXP C18 3 µm × 75 µm × 15 cm column chip) or a home-packed emitter column (Dr. Maish Reprosil C18 3 µm × 75 µm × 10 cm) as indicated in **Supplementary Table 2**. Buffer A was 0.1% formic acid in water; buffer B was 0.1% formic acid in ACN. The HPLC delivered an acetonitrile gradient over 120 min (2–35% buffer B over 85 min, 40–60% buffer B over 5 min, 60–90% buffer B over 5 min, hold buffer B at 90% 8 min and return to 2% B at 105 min). The DDA parameters for acquisition on the TripleTOF 5600 were 1 MS scan (250 ms; mass range 400–1,250) followed by (i) up to 50 MS/MS scans (50 ms each), (ii) up to 20 MS/MS scans (100 ms each) or (iii) up to 10 MS/MS scans (100 ms each) as indicated in **Supplementary Table 2**. Candidate ions with a charge state between 2 and 5 and counts above a minimum threshold of 200 counts per second were isolated using a window of 0.7 a.m.u. Previous candidate ions were dynamically excluded for 20 s with a 50-mDa window. The SWATH setup was essentially as in Gillet *et al.*[18], with the same chromatographic conditions used as in the DDA run described above, and with a 50-ms MS1 scan followed by 32 × 25-a.m.u. isolation windows covering the mass range of 400–1,250 a.m.u. (cycle time of 3.25 s); an overlap of 1 Da between SWATH was preselected. The collision energy for each window was set independently as defined by $CE = 0.06 \times m/z + 4$, where m/z is the center of the each window, with a spread of 15 eV performed linearly across the accumulation time. For the GRK6 experiments, the retention times were realigned according to landmark peptides to correct for the different chromatographic systems employed in this experimental set. The iTRAQ samples were acquired by DDA as described above (with the iTRAQ CE option applied)

using a packed-tip emitter system with direct injection, and up to 20 MS/MS scans were performed in each cycle.

Data-dependent acquisition processing for targeted extraction. We searched data generated by DDA against the human complement of the UniProt release 8.8 database containing 40,476 sequences using ProteinPilot AB Sciex Beta 4.1.46, revision 460. Searches were performed using ProteinPilot's standard "rapid search" parameter space that includes common modifications as part of the search. The search is undertaken using the Paragon search engine (v.4.0.0.0). The specific nature of this search engine and its mode of operation are described elsewhere[41]. Raw data for each experimental set were searched in a single batch (the description of the files is in **Supplementary Table 2**) to create a results file that was subsequently used for library generation.

Library generation. For each set of experiments (defined as per **Supplementary Table 2**), a specific library of precursor masses and fragment ions was created and used for subsequent SWATH processing. ProteinPilot result files were processed to extract matched peptide IDs and the matched ions from the original input spectra. The matched spectra were filtered to produce a list of parent masses and fragment masses and intensities to be used for SWATH processing.

Filtering removed peptide redundancy and identified the optimal spectrum for each peptide according to the following scheme. (i) Spectra were grouped on the basis of unique peptide identification; (ii) the grouped spectra were ranked according to identification confidence in ProteinPilot; (iii) the highest-confidence identification closest to the LC parent-ion peak apex was selected (the chromatographic peak apex is estimated by ProteinPilot and is exported as the intensity of the peak); (iv) the highest ranked spectra were then reinterpreted and y and b ions identified; (v) a library entry was made from the y and b ions for each top-ranked unique peptide spectrum. No attempt was made to generate a consensus spectrum from all identifications of each peptide. The data within this library contained modified forms as well as peptides that were shared between different protein isoforms.

SWATH data file processing. Prior to data processing, peptides were selected automatically from the library using the following decision tree. (i) The extracted results from the ProteinPilot results file contains all identified unique peptides for a specific targeted protein. These unique peptides were ranked by the intensity of the MS1 precursor ion from the DDA analysis as estimated by the ProteinPilot software. (ii) Peptides that contained modifications and/or were shared between different protein entries/isoforms were excluded from selection. (iii) Peptides that were represented by multiple charge states in the list were collapsed to the charge state that had the most intense precursor ion in the DDA data. Up to 15 peptides were chosen per protein, and SWATH quantitation was attempted for all proteins in library files that were identified below 1% FDR from ProteinPilot searches.

Target fragment ions, up to a number specified by the user and typically 4 or 5, were automatically selected as follows. (i) Fragment ions for a selected peptide were ranked according to ion intensity. (ii) Ions higher in m/z than the y_4 fragment ion for each selected peptide were ranked highest. (iii) Ions within the SWATH isolation window were excluded from selection.

(iv) If insufficient target ions were found, ions lower than y_4 but outside of the SWATH window were chosen. (v) If there were still insufficient ions, then fragment ions from within the SWATH window region were chosen. Avoiding ions within the SWATH window as much as possible decreases potential interferences from unfragmented precursor ions.

The specifics of the scoring for the different peak groups will be described elsewhere (R.A. and S.T., unpublished data). In essence: (i) the fragment ions for each peptide were used to generate extracted ion chromatograms (XIC) from the SWATH experiment that contained the parent m/z. (ii) Peaks identified in the different XICs were aligned by the peak apex retention time, and peaks that aligned across the different XICs were marked as potential candidate peak groups. (iii) For each candidate peak group on the list, the overlap of the different XIC peaks was evaluated, as related fragment ions should have the same peak width, and those which did not have well-correlated peak widths were removed from the candidate list. Overlap was assessed by using the half-height width of the most intense fragment peak to define a time window and verifying that the apex value of the other fragments was within the window. (iv) All the remaining peak groups were scored according to proximity to the expected retention time for the eluting component determined from the DDA data acquired using the same chromatographic system. (v) The MS/MS spectra for the peak apex of each of the remaining peak group candidates were extracted. (vi) The extracted spectra were scored according to the isotopic state of the individual ions extracted in the MS/MS spectra. Those peak groups which contained measurements extracted from ^{13}C isotopes were scored lower. (vii) The MS/MS spectra were also scored on the basis of the mass accuracy (both absolute and median accuracy) of the extracted peaks. (viii) The individual peak group scores were a linear combination of all subscores and the peak group with the best score was taken forward.

Determination of a robust peak extraction cutoff. To select the peak group confidence threshold for automated extraction, we used a method based on mProphet[42] to determine the false detection of peak groups. In essence, each peptide had both a forward and a reverse (decoy) sequence extracted, and the decoy sequence scores were used to generate a median score value for the retention time region of each forward sequence. This median score was used to normalize the score values and generate a recomputed score that ranked. As this ranked score list contains both forward and reverse sequences, standard methods for determining false positive results can be used. Here we used data from the CDK4 WT data set (group 5) to evaluate the impact of varying FDR threshold selection on the CV values and the final fold-change calculations. As shown in **Supplementary Figure 8a**, the percentage of peptides with CV values ≤20% were strongly affected by a reduction in the FDR stringency for peak extraction, which is consistent with the fact that FDR thresholding properly acts to reduce noise. Surprisingly, however, initial FDR selection had only a minimal impact on the final results of the fold-change calculations (see below for methods), a result suggesting that robustness is built into the normalization process that weights down the 'bad' fragments/peptides (**Supplementary Fig. 8b**). Despite this robustness (the final list of the proteins passing the fold-change confidence thresholds in this study was virtually unaffected by

extracting at 1% FDR or 10% FDR), for some proteins there was a clear negative effect on the confidence scores associated with the 10% FDR extraction (**Supplementary Fig. 8c**). Therefore, we elected to use a consistent 1% extraction FDR threshold for all the analyses described in the main text.

Extraction of MS1 and comparative CV analyses. We extracted MS1 intensities for identified peptides directly from the ProteinPilot results by exporting the ProteinPilot group files as a peptide summary table that includes the expected precursor intensity. DDA peptides were filtered as follows: (i) the peptides should be in common to all three DDA runs (otherwise, the missing values drastically increase the variance); (ii) the peptides should have been identified with ID confidence ≥99% in at least one of the three runs; (iii) all peptides, including modified peptides, are considered; (iv) each charge state is considered as a separate instance for quantification; (v) instances of the same peptide (with same charge) are considered the same peptides if they are within ±5 min of the retention time window. This set of criteria led to 2,741 common peptides, including peptides with different charge state and modifications.

To best compare the MS1-DDA variance to that of SWATH, we used a subset of these peptides that was deemed most reproducible (unmodified and present in only one protein) and also detected in the SWATH analysis of the most similar samples, i.e., the DDA run and the first SWATH analysis for each replicate. The SWATH data were restricted to those peptides that had an FDR ≤1% in at least two samples (note that we are attempting to quantify only the top 400 proteins in this analysis), and this list was merged with the DDA peptides to identify common peptides and remove modified peptides. The resulting list contained 1,320 common peptides that were used to evaluate the CV values for the SWATH and the DDA-MS1 measurements.

iTRAQ data analysis. iTRAQ data were analyzed using ProteinPilot 4.2, and the default ProGroup algorithm iTRAQ processing parameters were used. After a rapid search against UniProt, protein iTRAQ ratios were exported and s.d. was calculated across the replicate data sets. To generate **Supplementary Figure 18**, we extracted quantitative information for proteins used in the SWATH measurements alongside their s.d.

Determination of signal-quality metrics. A signal-quality value was determined for all raw data extracted. For the purpose of this study, the area of the peak was used as a surrogate value for the signal-to-noise ratio. The values for each transition were normalized to a scale of 0–1.0, where a value of 1.0 corresponded to an intensity of >10^6. A sigmoidal distribution was used, and the inflection point of the curve was set to a value of 10^5. The signal-quality metric is used during the fold-change determination of the peptides and proteins.

Normalization of peak area data. In a previous study[13] that used SRM to monitor the changes in the GRB2 interactome induced by stimulation or drug treatment, we normalized all data to the expression of the GRB2 bait itself. This was possible, as a single cell line was used for all studies and GRB2 levels were invariant across all conditions. Here, by contrast, we profiled the interactions established by bait proteins expressed in independent cell lines.

Though a major strength of the expression system that we used is that the different alleles are expressed at a similar level, there are small variations in expression levels that preclude normalization to the bait level (when we did this analysis, proteins that nonspecifically interacted with the affinity matrix tended to be identified as varying). We and others have previously realized that many of the proteins detected in AP-MS are interacting nonspecifically with the affinity matrix but that these interactions are reproducibly detected, both qualitatively and quantitatively[38]. With this knowledge, we therefore opted to use a normalization method that is independent of the bait expression. As defined in ref. 13, the identification of features for the normalization of data is critical. In this study we used features that had intensity greater than 3,000 (peak area) for normalization by a method similar to that in ref. 43 but modified because mass spectrometry intensity data are linearly dependent on the amount of material present.

The same normalization scheme was used for each experiment set. The procedure starts by examining the measurement ratios in biological replicates as follows. (i) The ratio between the measurements for each feature in each pair of replicates is determined. (ii) The ratios are represented as a histogram and the delta of the most likely ratio to the zero point is taken for each sample comparison (**Fig. 1b**). These values represent the sample differences and are used for normalization of the data as described below. (iii) The width of the ratio histogram is determined and is used as an indication of pairwise sample similarity. Here a narrow histogram will represent a good similarity between the different samples. (iv) Measurement reproducibility is also determined from the histogram as the distance of the feature ratio to the peak apex of the histogram. **Figure 1c**, top subpanel, shows the ratio histograms for all samples compared to one WT sample before normalization.

The first stage of normalization adjusts the values for a set of replicates (here, for example, biological replicates for the CDK4 WT samples are adjusted separately from the CDK4 R24C or R24H) because these values should be most similar. For each set the best sample, as measured by overall reproducibility, is determined, and the values for all other samples are adjusted using the appropriate apex ratio. The result of this intermediate normalization step is represented by the middle subpanel in **Figure 1c**, which shows the resulting ratio histograms and indicates that replicates are now very similar. These data—referred to as the 'biological sample normalized data'—are then used to normalize between different experiments.

The second stage is normalization between the different experiment conditions, for example, wild type and a selected mutant, using the output from the first stage. We processed these data as described above to determine the normalization factor for each experimental condition applied to the biological sample normalized data, generating the final 'experimental normalized data'. The final result is represented in **Figure 1c**, bottom, which shows that the apex ratio between all samples is now unity.

Selection of the normalization method. The method used for normalization of the data (most likely ratio normalization, MLR) was compared to other recognized methods of data normalization, including total area sums (TAS) and normalization to bait protein. TAS is performed by summing the responses for each sample and then determining a ratio of each sample to the largest sum.

This ratio is used as a normalization factor for each sample. For normalization to a bait protein, the responses for the bait proteins are summed, and then the median ratio between the peptides is determined; this value is used to normalize all other measurements in each sample. **Supplementary Figure 33a** shows the differences on the resulting PCA analysis between sample grouping using TAS, normalization to the bait protein and MLR for an experimental data set from triplicate analyses of three bait proteins, in which one replicate for two of the baits had a much lower overall intensity. Although the normalization to the bait clearly fails in this case, there was an improvement with MLR over TAS in obtaining separation. This was most obvious when visualizing the ratio histograms after normalization (**Supplementary Fig. 33b**). As the primary aim of normalization is to minimize experimental variance, balancing the ratio histograms ensures that the variance has been minimized. The variance of the samples is defined as the range of the peak apexes of the ratio histograms. Here the issues associated with the normalization to the bait protein (substantial sample variance even after normalization) are clearly depicted. Although the TAS approach minimized this variance between samples, the two outliers (intensity wise) were still unaligned. By contrast, MLR was successful at minimizing the variance, even for these samples with a poor intensity response.

Note that in terms of the fold-change determination, although normalization of the data to the bait protein makes sense if the bait protein itself is expected to be a constant value (this was in fact the method we used for the analysis of the SRM data in a previous publication[13]), even small variations in the abundance of the bait protein across the samples strongly affected the results (essentially, boosting all contaminant proteins in the samples in which the bait was expressed to a lesser extent). Here, as seen in the western blots in **Figures 3b** and **4e** (and accompanying quantitative mass spectrometry analysis), though the WT and mutants CDK proteins were expressed at similar levels, these levels were not identical (the WT was expressed to a higher level than the mutants). This prevented us from using the bait normalization, which we had previously employed; MLR was not affected by these differences.

Determination of fold change of values. All of the raw data collected were used to provide an input to the fold-change determinations. In essence, the fold change of the protein was determined using the method reported in ref. 13. Data after normalization—experimental normalized data—are used for the fold-change determination. These data are treated in the following manner. (i) For each set of biological replicates, a table of weighted average areas is determined using the transition reproducibility values determined during normalization—'weighted area response'. (ii) Weighted analysis of variance is used to determine the likelihood of difference between the experimental test conditions. The output is in essence a *P* value as if a *t*-test were performed between the different experiments, but the use of weighted values better accounts for poor-quality values in the data being processed. (iii) The 'signal-quality values' and 'analysis of variance values' (from step ii) are used to determine the peptide fold-change values via a weighted-average fold-change calculation. (iv) A peptide signal-quality table is determined from the transition signal-quality table by calculation of the median signal quality for each set of transitions. (v) The peptide variance is determined by calculating

the summed weighted average for the transitions analysis of variance using the signal-quality table as the weighting factor for the individual transitions. (vi) A protein fold-change value is determined as described in Bisson *et al.*[13], with a slight modification: the protein value is again a weighted average using both the peptide signal quality (step iv) and the peptide variance (step v) values as weights (**Supplementary Note**).

As described before, the output of this fold-change determination is a fold change up and down for each protein and a confidence value as determined from the peptide variance and the peptide signal-quality values.

All calculations were performed in Matlab 2012 by executing custom coded algorithms and data exported either in figure format or as text.

Determination of data quality metrics. Data quality is determined for the transitions, peptides and proteins, and is used to reject lower-quality values from subsequent processing and display. (i) The transition quality matrix is determined by taking the maximum median value of the data in the transition reproducibility matrix as determined in the normalization of the data. (ii) The peptide quality matrix is determined by taking median value for the transition quality values. (iii) The protein quality is determined from the median of the individual peptide quality values.

Filter parameters for data visualization and figure generation. Data represented in all figures were generated using a series of custom algorithms executed within the Matlab environment. The output from these scripts were figures and tables representing the fold change and corresponding confidence values.

Although data were filtered primarily using a confidence threshold of ≥0.75, we also required a minimum $\log_{10}$(fold change) value of 0.2. This latter value is based on distributions of pairwise fold-change values for all measurements with confidence values <0.75 (i.e., most likely not changing) in the initial CDK4 mutant experiment that showed that ~95% of the $\log_{10}$(fold change) values were less than 0.2. Further, to ensure that each protein is represented by high-quality measurements, we required at least two peptides per protein and used signal-quality and reproducibility thresholds of 0.15 (determined from the appropriate histograms).

For the data presented in the main text figures, an additional filtering scheme, based on the fold-change calculations, was applied to ensure that only specific interactors for a bait are considered 'potentially modulated interactors'. Essentially, we applied two criteria: (i) the prey protein must have passed the confidence and fold-change thresholds as defined above and be upregulated in comparison to a set of negative-control samples processed in parallel (we consider any proteins passing the thresholds across the entire set of baits to be tested a 'specific interactor' for the bait); and (ii) pairwise comparisons between sequence variants and/or drug treatments are then performed, considering only the specific interactors, and the same thresholds (this time, up or down) are applied. Data resulting from only the second step (meaning without first ensuring that the proteins analyzed are noncontaminants) can be found in **Supplementary Figs. 20–22** and **30–32**; see also **Supplementary Figs. 34–39**); these values should be interpreted with caution, as the filtering of contaminants is less stringent.

The layout of the figures was also generated in Matlab and annotated in Illustrator: in the case of the complete data set representation for each experiment set, the rank is based on the global view where proteins are ranked by decreasing confidence of fold change across any two pairs.

The figures presented in the main text use the same filtering criteria and cutoffs and represent the fold-change data as a heat map generated (increasing ratios) using MultiExperiment Viewer v.4.8.1 (MeV; http://www.tm4.org/mev/).

Access to data. All mass spectrometry data as well as each of the steps of the analysis can be found at http://prohits-web.lunenfeld.ca/. Raw mass spectrometry files were also deposited in the MassIVE repository, housed in the Center for Computational Mass Spectrometry at UCSD (http://massive.ucsd.edu/ProteoSAFe/datasets.jsp); see **Supplementary Table 4** for IDs and links to each of the data sets.

39. Dunham, W.H. *et al.* A cost-benefit analysis of multidimensional fractionation of affinity purification-mass spectrometry samples. *Proteomics* **11**, 2603–2612 (2011).
40. Luke-Glaser, S. *et al.* CIF-1, a shared subunit of the COP9/signalosome and eukaryotic initiation factor 3 complexes, regulates MEL-26 levels in the *Caenorhabditis elegans* embryo. *Mol. Cell. Biol.* **27**, 4526–4540 (2007).
41. Shilov, I.V. *et al.* The Paragon Algorithm, a next generation search engine that uses sequence temperature values and feature probabilities to identify peptides from tandem mass spectra. *Mol. Cell. Proteomics* **6**, 1638–1655 (2007).
42. Reiter, L. *et al.* mProphet: automated data processing and statistical validation for large-scale SRM experiments. *Nat. Methods* **8**, 430–435 (2011).
43. Bolstad, B.M., Irizarry, R.A., Astrand, M. & Speed, T.P. A comparison of normalization methods for high density oligonucleotide array data based on variance and bias. *Bioinformatics* **19**, 185–193 (2003).